

# Assumed Strain Finite Elements for Reissner-Mindlin Plates

G. Castellazzi, P. Krysl

*University of California, San Diego, 9500 Gilman Dr #0085, La Jolla, CA 92093-0085,*

*Email: gicastellazzi@ucsd.edu, pkrysl@ucsd.edu*

*Keywords:* Reissner-Mindlin plate, finite element, shear locking, assumed strain, weighted residual, nodal quadrature.

This paper deals with a new family of displacement based finite elements with nodal integration for Reissner-Mindlin plates. The Reissner-Mindlin model describes the deformation field of a plate in response to transverse loading in terms of the displacement of the midplane and the rotations of the fibers normal to the midplane. Finite elements are often used as discretizations, but although they are seemingly very reasonable choices, they can result in poor behavior for thin plates, which is termed shear locking. Many remedies have been proposed over the years: the literature is too extensive to be reviewed here.

We present here an extension of the assumed-strain finite element technique presented in [2] where a successful approach to cure this trouble is proposed. The starting point of the technique is the method of weighted residuals where the weakly enforced equations roughly correspond to a strain-displacement variational approach [4].

The weak kinematic equation (the strain-displacement relationship) is considered separately from the weak balance equation, it is satisfied a priori and yields the assumed-strain operators via nodal integration. The derived strain-displacement operators lead to just the right number of constraints to avoid shear locking as the thickness of the plate decreases. Both the actual (generalized) strains and the test strains are derived using special operators. This is the point where the nodal quadrature is enabled by allowing for uniquely defined (assumed) strains at the nodes.

The nodal-integration rules are available for both triangular and quadrilateral elements, and yield approximations for meshes consisting of an arbitrary mix of triangles and quadrilaterals.

Importantly, the degrees of freedom are only the primitive displacement variables: transverse displacements and rotations at the nodes.

## 1 SUMMARY OF THE GOVERNING EQUATIONS

Consider a plate referred to the following Cartesian coordinate frame:

$$V = \{(x, y, z) \in \mathbb{R}^3 | z \in [-t/2; t/2], (x, y) \in A \in \mathbb{R}^2\}, \quad (1)$$

where  $A$  is the area of the plate, and  $t$  is the thickness of the plate. The boundary of the plate is  $C = \partial A$ . The 3-D displacement is denoted  $\mathbf{u}$  and its Cartesian components are

$$u_x = z\varphi_y, \quad u_y = -z\varphi_x, \quad u_z = w, \quad (2)$$

where  $\varphi_x = \varphi_x(x, y)$  and  $\varphi_y = \varphi_y(x, y)$  are the rotations of the transverse normal about the Cartesian axes  $x$  and  $y$ , and  $w = w(x, y)$  is the deflection. The functions  $\varphi_x$ ,  $\varphi_y$ , and  $w$  are the unknown fields in the plate bending problem, and we can conveniently express the three-dimensional displacement vector in terms of the mixed-component vector of the generalized displacements  $\tilde{\mathbf{u}}$

$$[\tilde{\mathbf{u}}] = [w, \varphi_x, \varphi_y]^T, \quad \mathbf{u} = \mathbf{S}\tilde{\mathbf{u}}, \quad (3)$$

Table 1: Summary of the equations for the Reissner-Mindlin plate theory. BC= boundary condition. With some abuse of notation we write the boundary conditions as applying for each component (normal, tangential, vertical) for either the essential or the natural kind at each point of the curve  $C$ .

Type	Holds where	Equation
Kinematics	in $A$	$\boldsymbol{\kappa} = \mathcal{B}^b \tilde{\mathbf{u}}, \quad \boldsymbol{\gamma} = \mathcal{B}^s \tilde{\mathbf{u}}$
Constitutive	in $A$	$\mathbf{m} = \frac{t^3}{12} \mathbf{D}^b \boldsymbol{\kappa}, \quad \mathbf{s} = tkG\boldsymbol{\gamma}$
Balance	in $A$	$\mathcal{B}^{bT} \mathbf{m} + \mathcal{B}^{sT} \mathbf{s} + t\bar{\mathbf{b}} = \rho \mathbf{I} \ddot{\mathbf{u}}$
Essential BC	on $C$	$\varphi_n = \bar{\varphi}_n$ or $\varphi_s = \bar{\varphi}_s$ or $w = \bar{w}$
Natural BC	on $C$	$m_{nn} = \bar{m}_{nn}$ or $m_{ns} = \bar{m}_{ns}$ or $s_{nz} = \bar{s}_{nz}$

where we introduced the shifter  $\mathbf{S}$  as defined next.

The bending symmetric gradient operator is defined as  $\mathcal{B}^{bz} = z\mathcal{B}^b$ , and the shear symmetric gradient operator is defined as  $\mathcal{B}^s$ , where

$$\mathcal{B}^b = \begin{bmatrix} 0 & 0 & \partial/\partial x \\ 0 & -\partial/\partial y & 0 \\ 0 & -\partial/\partial x & \partial/\partial y \end{bmatrix}, \quad \mathcal{B}^s = \begin{bmatrix} \partial/\partial x & 0 & 1 \\ \partial/\partial y & -1 & 0 \end{bmatrix}, \quad \mathbf{S} = \begin{bmatrix} 0 & 0 & z \\ 0 & -z & 0 \\ 1 & 0 & 0 \end{bmatrix} \quad (4)$$

and is used to produce bending and shear strains

$$\boldsymbol{\epsilon}^b = z\mathcal{B}^b \tilde{\mathbf{u}} = z\boldsymbol{\kappa}, \quad \boldsymbol{\epsilon}^s = \boldsymbol{\gamma} = \mathcal{B}^s \tilde{\mathbf{u}}, \quad (5)$$

The bending and the shear stresses are generated by the constitutive equation of plane stress

$$\boldsymbol{\sigma}^b = \mathbf{D}^b \boldsymbol{\epsilon}^b = z\mathbf{D}^b \boldsymbol{\kappa}, \quad \boldsymbol{\sigma}^s = \mathbf{D}^s \boldsymbol{\epsilon}^s = kG\boldsymbol{\epsilon}^s = kG\boldsymbol{\gamma}. \quad (6)$$

where in general  $\mathbf{D}^b$  and  $\mathbf{D}^s$  describes an anisotropic material. The balance equation may be written using the above operators as

$$\mathcal{B}^{bzT} \boldsymbol{\sigma}^b + \mathcal{B}^{sT} \boldsymbol{\sigma}^s + \bar{\mathbf{b}} = \rho \mathbf{S}^T \ddot{\mathbf{u}} = \rho \mathbf{S}^T \mathbf{S} \ddot{\mathbf{u}}. \quad (7)$$

We assume  $[\bar{\mathbf{b}}] = [0, 0, \bar{b}_z(x, y)]^T$  for simplicity. Integrating the balance equation through the thickness of the plate obtains

$$\mathcal{B}^{bT} \mathbf{m} + \mathcal{B}^{sT} \mathbf{s} + t\bar{\mathbf{b}} = \rho \mathbf{I} \ddot{\mathbf{u}}, \quad (8)$$

where we define as usual

$$\mathbf{I} = \begin{bmatrix} t & 0 & 0 \\ 0 & t^3/12 & 0 \\ 0 & 0 & t^3/12 \end{bmatrix}, \quad (9)$$

and the resultants

$$\mathbf{m} = \int_{-t/2}^{t/2} z\boldsymbol{\sigma}^b dz = \frac{t^3}{12} \mathbf{D}^b \boldsymbol{\kappa}, \quad \mathbf{s} = \int_{-t/2}^{t/2} \boldsymbol{\sigma}^s dz = tkG\boldsymbol{\gamma}. \quad (10)$$

The equations for the Reissner-Mindlin theory are summarized in Table 1.

## 2 WEIGHTED RESIDUAL FORMULATION

The weighted residuals, where the weakly enforced equations roughly correspond to a strain-displacement variational approach [4], is the starting point of the method. Thus, the various equations in Table 1 will be enforced either strongly (constitutive equation, essential boundary condition), or weakly (kinematic equation, balance equation, and natural boundary condition). We recall now briefly the construction of the weak form of the Reissner-Mindlin governing equations used in [2].

We shall assume, as is usual, that the finite element nodes carry the degrees of freedom,  $w_i$ ,  $\varphi_{xi}$ ,  $\varphi_{yi}$  associated with node  $i$ . This is equivalent to  $2N_q$  algebraic constraints between the  $3N_n$  parameters  $w_i, \varphi_{xi}, \varphi_{yi}$ , where  $N_q$  is the number of quadrature points and  $N_n$  is the number of nodes.

Quadrature at integration points which correspond one-to-one to the nodes (that is  $N_q = N_n$ ) may yield exactly the right number of constraints, provided these are linearly independent.

However, nodal quadrature cannot process the integrands from the individual elements connected at the node directly, since each contributing basis function derivative will be multi-valued at the node (discontinuous across the element edges).

For the purpose of nodal quadrature, the basis functions derivatives (or, equivalently, the strains) should be therefore computed using a special strain-displacement operator, and so we are led to consider an assumed-strain method.

The residual equations are

$$r_{BC} = \int_A \left[ -(\mathcal{B}^b \tilde{\eta})^T \mathbf{m} - (\mathcal{B}^s \tilde{\eta})^T \mathbf{s} + t \tilde{\eta}^T \bar{\mathbf{b}} - \varrho \tilde{\eta}^T \mathbf{I} \ddot{\mathbf{u}} \right] dA + r_C = 0. \quad (11)$$

for the balance equation residual, where  $r_C$  is the natural boundary condition residual, and

$$r_{Kb} = \int_A \boldsymbol{\lambda}^{bT} \mathbf{D}^b (\boldsymbol{\kappa} - \mathcal{B}^b \tilde{\mathbf{u}}) dA = 0, \quad r_{Ks} = \int_A \boldsymbol{\lambda}^{sT} \mathbf{D}^s (\boldsymbol{\gamma} - \mathcal{B}^s \tilde{\mathbf{u}}) dA = 0, \quad (12)$$

for the kinematic equation residual. Here  $\tilde{\eta}$  is the test function (generalized displacement, as indicated by the tilda), which is assumed to vanish along the portions of boundary where essential boundary conditions are prescribed, as customarily done to eliminate the unknown reactions:  $[\tilde{\eta}]_i = 0$  where  $i^{\text{th}}$  component of the generalized displacement is prescribed on  $C$ . The test functions  $\boldsymbol{\lambda}^b$  and  $\boldsymbol{\lambda}^s$  have the meaning of generalized strains (curvatures and shear deformations).

The balance residual is manipulated in a standard way to shift one spatial derivative from the stress resultants to the test function. The two residual equations, (11) and (12), are equivalent to a certain extent to a strain-displacement variational statement [4] where they are merged into a single residual equation. In the present context we keep the two kinds of residual separate. We will use the weak kinematic equation to derive the assumed-strain operator, thereby satisfying this equation a priori: both the actual (generalized) strains  $\boldsymbol{\kappa}, \boldsymbol{\gamma}$  and the test strains  $\boldsymbol{\lambda}^b, \boldsymbol{\lambda}^s$ , are derived using special operators

$$\boldsymbol{\lambda}^b = \bar{\mathcal{B}}^b \tilde{\eta}, \quad \boldsymbol{\kappa} = \bar{\mathcal{B}}^b \tilde{\mathbf{u}}, \quad \boldsymbol{\lambda}^s = \bar{\mathcal{B}}^s \tilde{\eta}, \quad \boldsymbol{\gamma} = \bar{\mathcal{B}}^s \tilde{\mathbf{u}} \quad (13)$$

and we may note the resemblance to the original B-bar technique [5], and the kinematic residuals resulting in

$$\begin{aligned} r_{Kb} &= \int_A (\bar{\mathcal{B}}^b \tilde{\eta})^T \mathbf{D}^b (\bar{\mathcal{B}}^b \tilde{\mathbf{u}} - \mathcal{B}^b \tilde{\mathbf{u}}) dA = 0, \\ r_{Ks} &= \int_A (\bar{\mathcal{B}}^s \tilde{\eta})^T \mathbf{D}^s (\bar{\mathcal{B}}^s \tilde{\mathbf{u}} - \mathcal{B}^s \tilde{\mathbf{u}}) dA = 0. \end{aligned} \quad (14)$$

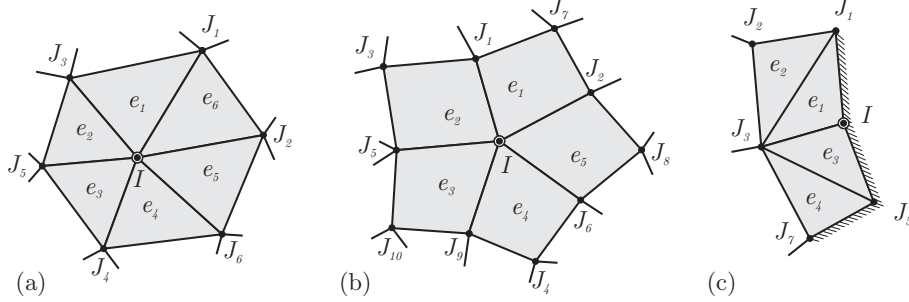


Figure 1: Nodal patch illustrated on: a three-node triangular mesh (a); a four-node quadrilateral mesh (b); and a three-node triangular mesh with boundary conditions (c).

### 3 ASSUMED-STRAIN OPERATORS

In this section nodal quadrature is enabled by allowing for uniquely defined (assumed) strains at the nodes. At this point, the assumed-strain operators  $\overline{\mathbf{B}}^b, \overline{\mathbf{B}}^s$  are not known, but can be *derived* from the condition that they will make the kinematic residuals (14) identically zero. The process will be the same for both  $\overline{\mathbf{B}}^b$  and  $\overline{\mathbf{B}}^s$ . Consequently we will describe the construction of  $\overline{\mathbf{B}}^s$ , with the adjustments necessary to construct  $\overline{\mathbf{B}}^b$  implied.

We introduce the finite element approximation:  $\tilde{\mathbf{u}} = \sum_I N_I \tilde{\mathbf{u}}_I$ , and  $\tilde{\boldsymbol{\eta}} = \sum_I N_I \tilde{\boldsymbol{\eta}}_I$ . The discrete kinematic weighted residual equation becomes

$$\sum_{I,J} \tilde{\boldsymbol{\eta}}_I^T \left( \int_A \overline{\mathbf{B}}_I^{sT} \mathbf{D}^s (\overline{\mathbf{B}}_J^s - \mathbf{B}_J^s) dA \right) \tilde{\mathbf{u}}_J = 0, \quad (15)$$

where we have introduced matrices  $\mathbf{B}_J^s = \mathcal{B}^s(N_J)$ , and the nodal strain-displacement matrices  $\overline{\mathbf{B}}_I^s$ , as not yet unspecified, that are used to produce the assumed strains as

$$\boldsymbol{\gamma} = \sum_I \overline{\mathbf{B}}_I^s \tilde{\mathbf{u}}_I. \quad (16)$$

Evidently, the  $\tilde{\boldsymbol{\eta}}_I$  are entirely arbitrary, and furthermore we would not wish the matrices  $\overline{\mathbf{B}}_I^s$  to depend on the solution  $\tilde{\mathbf{u}}_J$ . Consequently, the vanishing of the integrals

$$\int_A \overline{\mathbf{B}}_I^{sT} \mathbf{D}^s (\overline{\mathbf{B}}_J^s - \mathbf{B}_J^s) dA = \mathbf{0}, \quad \forall J, \quad (17)$$

is implied for fixed  $I$ . Refer to Figure 1 for an illustration that provide a better interpretation of the indices. For the index  $I$  fixed, we note that in order to formulate strictly local operations, we should only consider the strain-displacement matrices  $\mathbf{B}_J^s$  defined within the elements  $e_r, r = 1, \dots, 6$  connected to node  $I$ . The index  $J$  then ranges over  $J = J_q, q = 1, \dots, 6$  and  $J = I$ . Therefore, we replace  $\forall J$  in (17) with the limited range  $J \in \text{nodes}(\text{elems}(I))$ ; the term  $\text{nodes}(e)$  refers to the nodes of the element  $e$ , the term  $\text{elems}(I)$  refers to the elements connected to the node  $I$ , and the term  $\text{nodes}(\text{elems}(I))$  refers to the union of the nodes of the elements connected to the node  $I$ . Thus, we will work with the integrals

$$\int_A \overline{\mathbf{B}}_I^{sT} \mathbf{D}^s (\overline{\mathbf{B}}_J^s - \mathbf{B}_J^s) dA = \mathbf{0}, \quad J \in \text{nodes}(\text{elems}(I)), \quad (18)$$

for any fixed node  $I$ .

Next, numerical quadrature at the nodes is introduced in the area integrals. For the two element types that we consider in this section, the nodal quadrature rules are easily specified as

$$\int_A (\bullet)(\mathbf{x}) \, dA \approx \sum_e \sum_{K \in \text{nodes}(e)} (\bullet)(\mathbf{x}_K) \mathcal{J}(\mathbf{x}_K) W_K, \quad (19)$$

where  $e$  ranges over all the elements in the mesh,  $K$  ranges over all the quadrature points in the element (in this case, the quadrature points coincide with the nodes: three or four for the two simplest element shapes),  $\mathbf{x}_K$  is the location of the quadrature point (node),  $\mathcal{J}(\mathbf{x}_K)$  is the Jacobian of the isoparametric mapping, and  $W_K$  is the weight of the quadrature point.

Table 2 defines the quadrature rules for the element formulations discussed in this paper. The seven-node triangle, it can be described as the basic six-node triangle with one “node” associated with a relative displacement degree of freedom, bubble function [3]. As suggested in [2] an attractive possibility is to eliminate the seventh node entirely by setting the bubble basis function to be identically zero (and suppressing all degrees of freedom associated with the seventh node). The result is a *six-node* element used with a *seven-point integration rule* (of Table 2). Note that the centroid integration point is never associated with an active node, and belongs to one and only one element, and consequently it is just a regular integration point with no averaging operations involved. The resulting scheme is referred to as NIP-T7. Here the same scheme is used for the nine-node quadrilateral element. In the following developments, we assume that  $I$  is one particular fixed node. Using numerical quadrature, the integral (18) is replaced with this double sum

$$\sum_e \sum_{K \in \text{nodes}(e)} \mathcal{J}(\mathbf{x}_K) W_K \bar{\mathbf{B}}_I^{sT} \mathbf{D}^s(\mathbf{x}_K) [\bar{\mathbf{B}}_J^s - \mathbf{B}_J^s(\mathbf{x}_K)] = \mathbf{0}, \quad J \in \text{nodes}(\text{elems}(I)), \quad (20)$$

where  $e$  ranges over all the elements in the mesh. The sum over all the elements implies a mesh-wide operation. Quite reasonably, we will try to avoid this. Reversing the order in which we apply the double summation, with  $K$  ranging over all the nodes in the mesh, we obtain

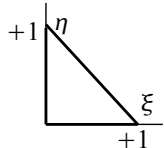
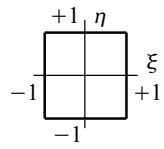
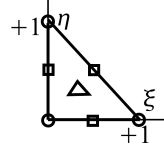
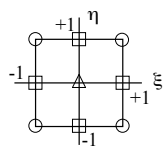
$$\sum_K \sum_{e \in \text{elems}(K)} \mathcal{J}(\mathbf{x}_K) W_K \bar{\mathbf{B}}_I^{sT} \mathbf{D}^s(\mathbf{x}_K) [\bar{\mathbf{B}}_J^s - \mathbf{B}_J^s(\mathbf{x}_K)] = \mathbf{0}, \quad J \in \text{nodes}(\text{elems}(I)). \quad (21)$$

Finally, for efficiency reasons the integration points should be independent. Therefore, we will require the vanishing of each of the terms in the above sum separately

$$\sum_{e \in \text{elems}(K)} \mathcal{J}(\mathbf{x}_K) W_K \bar{\mathbf{B}}_I^{sT} \mathbf{D}^s(\mathbf{x}_K) [\bar{\mathbf{B}}_J^s - \mathbf{B}_J^s(\mathbf{x}_K)] = \mathbf{0}, \quad J \in \text{nodes}(\text{elems}(I)). \quad (22)$$

for all integration points  $K$ . The matrices  $\mathbf{B}_J^s(\mathbf{x}_K)$  and the Jacobian  $\mathcal{J}(\mathbf{x}_K)$  are multi-valued at node  $K$ , depending on which element these quantities are evaluated at the node  $K$ . The constitutive matrix  $\mathbf{D}^s(\mathbf{x}_K)$  is assumed to be single-valued at  $\mathbf{x}_K$ . This would not be the case for points  $\mathbf{x}_K$  located at a multi-material interface, and such possibility is discussed in the remarks below. Note

Table 2: Nodal quadrature rule for the three-node triangle and the four-node quadrilateral and the seven-node triangle [3] and the nine-node quadrilateral .

Type	Parametric coordinates	Weights $W_K$
Three-node triangle		$\frac{1}{3}, \frac{1}{3}, \frac{1}{3}$
Four-node quadrilateral		1, 1, 1, 1
Seven-node triangle		$\bigcirc : \frac{1}{40}, \square : \frac{1}{15}, \triangle : \frac{9}{40}$
Nine-node quadrilateral		$\bigcirc : \frac{1}{9}, \square : \frac{4}{9}, \triangle : \frac{16}{9}$

that  $\bar{\mathbf{B}}_I^s$  and  $\bar{\mathbf{B}}_J^s$  are element-independent. Therefore, by rewriting (22) as

$$\begin{aligned}
 & \sum_{e \in \text{elems}(K)} \mathcal{J}(\mathbf{x}_K) W_K \bar{\mathbf{B}}_I^{sT} \mathbf{D}^s(\mathbf{x}_K) \left[ \bar{\mathbf{B}}_J^s - \mathbf{B}_J^s(\mathbf{x}_K) \right] = \\
 & = \bar{\mathbf{B}}_I^{sT} \mathbf{D}^s(\mathbf{x}_K) \sum_{e \in \text{elems}(K)} \mathcal{J}(\mathbf{x}_K) W_K \left[ \bar{\mathbf{B}}_J^s - \mathbf{B}_J^s(\mathbf{x}_K) \right] = \\
 & = \bar{\mathbf{B}}_I^{sT} \mathbf{D}^s(\mathbf{x}_K) \left[ \bar{\mathbf{B}}_J^s \sum_{e \in \text{elems}(K)} \mathcal{J}(\mathbf{x}_K) W_K - \sum_{e \in \text{elems}(K)} \mathcal{J}(\mathbf{x}_K) W_K \mathbf{B}_J^s(\mathbf{x}_K) \right] = \mathbf{0},
 \end{aligned} \tag{23}$$

we can conclude that the expression in the brackets must vanish, yielding

$$\bar{\mathbf{B}}_J^s \sum_{e \in \text{elems}(K)} \mathcal{J}(\mathbf{x}_K) W_K - \sum_{e \in \text{elems}(K)} \mathcal{J}(\mathbf{x}_K) W_K \mathbf{B}_J^s(\mathbf{x}_K) = \mathbf{0}. \tag{24}$$

This finally leads to the definition of the assumed-strain nodal matrix as a weighted average of the elemental strain-displacement matrices

$$\bar{\mathbf{B}}_J^s = \frac{\sum_{e \in \text{elems}(K)} \mathcal{J}(\mathbf{x}_K) W_K \mathbf{B}_J^s(\mathbf{x}_K)}{\sum_{e \in \text{elems}(K)} \mathcal{J}(\mathbf{x}_K) W_K}. \tag{25}$$

Thus, constructing the nodal strain-displacement matrices as averages of the strain-displacement matrices from the connected elements will satisfy the kinematic residual statement, enabling nodal quadrature in the process.

#### 4 NUMERICAL EXAMPLES

In this section, the performance of the described elements, is numerically verified on some standard test problems. The solutions obtained are compared with those from other quadrilateral and triangular elements available in literature.

##### 4.1 Square plate with uniform load: moments

A square plate of side length  $L$ , under uniformly distributed transverse load  $b_z = 1$ , is herein considered. Clamped condition is considered, imposing:  $w = \varphi_x = \varphi_y = 0$ . The analysis is carried out for three different aspect ratio:  $L/t = 10$ ,  $L/t = 100$  and  $L/t = 1000$  using various regular mesh. The following properties are assumed:  $E = 3 \times 10^6$ ,  $\nu = 0.3$  and  $k = \frac{5}{6}$ . For symmetry, only one quarter of the plate is modeled. Tables 3 and Figure 2 presents the displacement results at the centre of the clamped plate, together with the Energy values [6]–[7] and the bending moments visualized as raised surfaces.

Table 3: Computed displacement and energy for  $t = 1/10$ ,  $t = 1/100$  and  $t = 1/1000$  for a  $16 \times 16$  discretization. The displacement values are scaled by a factor of  $10^5$ ,  $10^{-2}$ ,  $10^{-1}$  respectively and the energy values are scaled by a factor of  $10^3$ ,  $10^3$  and  $10^9$  respectively.

N. elements	NIP-T3		NIP-Q4		NIP-T7		NIP-Q9	
	$w$	$E$	$w$	$E$	$w$	$E$	$w$	$E$
1/10	0.54914	0.45939	0.54670	0.45687	0.54770	0.45539	0.54767	0.45539
Ref. Sol.	$w_{ex} = 0.5477 \times 10^{-5}$		$E_{ex} = 0.4554 \times 10^{-3}$					
1/100	0.46267	0.35837	0.46063	0.35647	0.46124	0.35489	0.46147	0.35514
Ref. Sol.	$w_{ex} = 0.4614 \times 10^{-2}$		$E_{ex} = 0.35516 \times 10^3$					
1/1000	0.46174	0.35729	0.45973	0.35542	0.45849	0.35191	0.46056	0.35409
Ref. Sol.	$w_{ex} = 0.4605 \times 10$		$E_{ex} = 0.3541 \times 10^9$					

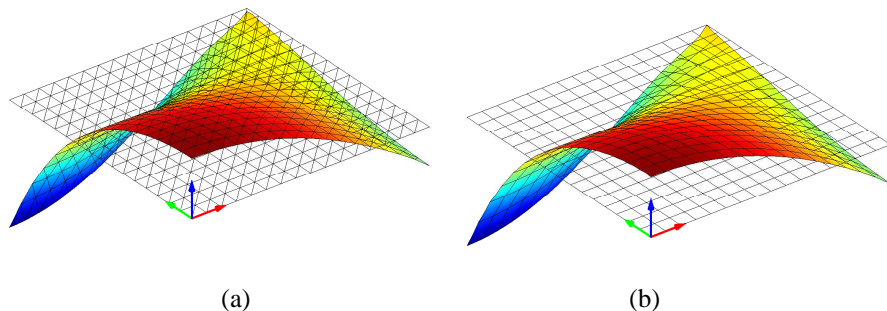


Figure 2: Clamped square plate under uniform load with  $t = 1/1000$ . Bending moments visualized as raised surfaces: (a) triangular T7 element; (b) quadrilateral Q9 element. Results for model for 16 element edges per side.

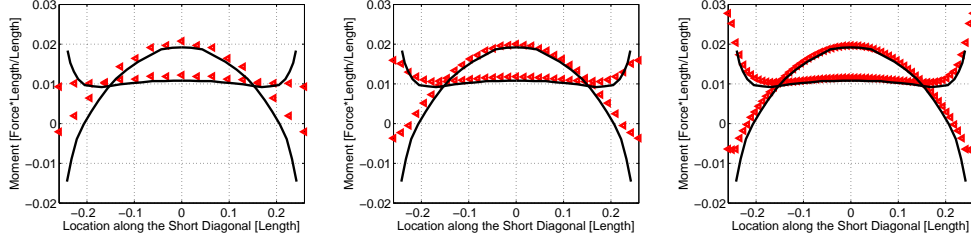


Figure 3: Rhombic plate  $L/t = 100$  with  $\beta = 30^\circ$ . Moments along the short diagonal. Results for model NIP-aT3, for 16, 32, and 64 element edges per side.

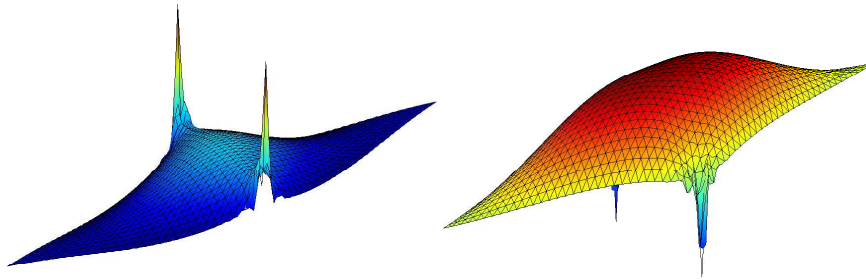


Figure 4: Rhombic plate  $L/t = 100$  with  $\beta = 30^\circ$ . Bending moments visualized as raised surfaces. Results for model NIP-aT7, for 32 element edges per side.

#### 4.2 Simply-supported rhombic ( $\beta = 30^\circ$ ) plate with uniform load: moments

The challenging problem of the highly skewed rhombic plate (skew angle  $\beta = 30^\circ$ ) is explored using the results of the convergence study [1]. The properties are: Young's modulus  $E = 30 \times 10^3$ , Poisson ratio  $\nu = 0.3$ , side length  $L = 1$ , thickness  $t = L/100$ , transverse uniform load of 1.0 units – all data in consistent units. The boundary condition is SS1:  $w = 0$ . The definitive 3-D elasticity study of this plate [1] provides the asymptotic solution. Convergence in the energy of deformation is assessed relative to several reference solutions. The following meshes are used in combination with the present formulations: NIP-Q4 and NIP-Q9 (structured quadrilateral mesh), NIP-T3 and NIP-T7 (structured triangular mesh produced from the quadrilaterals by bisection along the long diagonal).

In Figure 3 are reported the representation of the principal bending moments along the short diagonal for the triangular model NIP-T3. Figure 4 visualizes analogous results for the model NIP-T7 as surfaces raised into the third dimension above the plate. The approximations of the infinite moments at the obtuse corner shown as spikes. Note that these results are not postprocessed—the nodal moments are computed directly using the curvatures from Equation (13). Figure 5 reports the convergence in energy for  $L/t = 100$  (normalized by  $0.2655085 \times 10^{-4}$  from Reference [1])

#### 4.3 Clamped circular plate loaded with a central vertical force

The response of the present models is studied for the configuration of a clamped circular plate of radius  $R$ , with a central concentrated load, and for thickness to span ratio of 1/1000. Only one quadrant is modeled with appropriate symmetry boundary conditions. The present quadrilateral NIP-



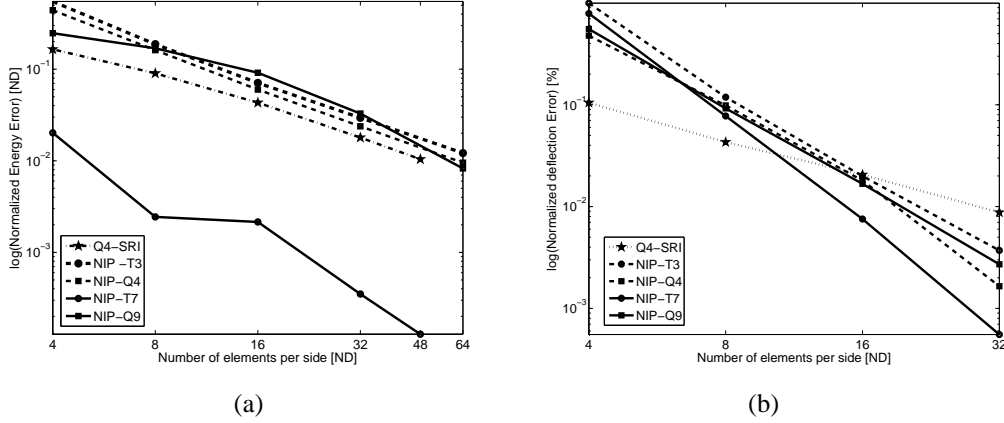


Figure 5: (a) Rhombic plate with  $\beta = 30^\circ$ . Convergence in energy for  $L/t = 100$  (normalized by  $0.2655085 \times 10^{-4}$  from Reference [1]); (b) Clamped circular plate loaded with a central vertical force: convergence in the normalized central point deflection

Q4 and NIP-Q9 and triangle NIP-T3 and NIP-T7 are compared with the Q4-SRI. The parameters are: Young's modulus  $E = 2.1 \times 10^6$ , Poisson ratio  $\nu = 0.3$ , radius  $R = 20$ .

Convergence in the normalized central point deflection (which in this case is equivalent to convergence in the energy) is reported in Figure 5(b). On the other hand, all the present models show robust convergence rates, approximately 2.5 for the NIP-T3, and the NIP-Q4 and NIP-Q9, and approximately 3.5 for the NIP-T7. This may be compared with the convergence rate of approximately 1 for the SRI.

## CONCLUSIONS

An extension to high order elements of our technique, recently proposed, has been presented, completing a new family of assumed-strain finite element for shear-deformable (Reissner-Mindlin) plates.

Weighted residual method (reminiscent of the strain-displacement functional) was used to enforce weakly the balance equation with the natural boundary condition and, separately, the kinematic equation (the strain-displacement relationship). The kinematic weighted residual serves as a condition from which strain-displacement operators were derived via nodal integration, for linear triangles, for quadrilaterals, and also for quadratic triangles and quadrilateral. The degrees of freedom employed were only the primitive variables: transverse displacements and rotations at the nodes. A straightforward constraint count can partially explain the insensitivity of the resulting finite element models to locking in the thin-plate limit. Numerical examples were used to illustrate the performance with particular attention to resultants representation.

## References

- [1] I. Babuška and T. Scapolla. Benchmark computation and performance evaluation for rhombic plate bending problem. *International Journal for Numerical Methods in Engineering*, 28:155–179, 1989.
- [2] G. Castellazzi and P. Krysl. Displacement-based Finite Elements with Nodal Integration for

Reissner-Mindlin Plates. *International Journal for Numerical Methods in Engineering*, Published - Early view, 2009.

- [3] G. C. Cohen. *Higher-order numerical methods for transient wave equation*. Springer, 2002.
- [4] CA Felippa. On the original publication of the general canonical functional of linear elasticity. *Journal of Applied Mechanics-Transactions of the ASME*, 67(1):217 – 219, 2000.
- [5] TJR Hughes. Generalization of selective integration procedures to anisotropic and non-linear media. *International Journal for Numerical Methods in Engineering*, 15(9):1413 – 1418, 1980.
- [6] T Scapolla and L Della Croce. Combining hierarchic high order and mixed-interpolated finite elements for reissnermindlin plate problems. *Computer Methods in Applied Mechanics and Engineering*, 116(1-4):185–192, 1994.
- [7] S. Timoshenko and S. Woinowsky-Krieger. *Theory of plates and shells*. McGraw-Hill, 1959.